Research Article

Biochemical characterization of the skeletal matrix of the massive coral, *Porites australiensis* - The saccharide moieties and their localization

Takeshi Takeuchi*[1], Laurent Plasseraud[2], Isabelle Ziegler-Devin[3], Nicolas Brosse[3], Chuya Shinzato[1,4], Noriyuki Satoh[1], and Frédéric Marin[5]

[1] Marine Genomics Unit, Okinawa Institute of Science and Technology Graduate University, Onna, Okinawa 904-0495, Japan

[2] Institut de Chimie Moléculaire de l'Université de Bourgogne, UMR CNRS 6302, Faculté des Sciences Mirande, Université de Bourgogne - Franche-Comté (UBFC), Dijon, France

[3] LERMAB, Faculté des Sciences & Technologies - Campus Aiguillettes, Université de Lorraine, Vandœuvre-Lès-Nancy, France.

[4] Department of Marine Bioscience Atmosphere and Ocean Research Institute, The University of Tokyo, Kashiwanoha, Kashiwa-shi, Chiba 277-8564, Japan

[5] UMR CNRS 6282 Biogéosciences, Bâtiment des Sciences Gabriel, Université de Bourgogne - Franche-Comté (UBFC), Dijon, France

***Corresponding author**

Takeshi Takeuchi: t.takeuchi@oist.jp

Abstract

To construct calcium carbonate skeletons of sophisticated architecture, scleractinian corals secrete an extracellular skeletal organic matrix (SOM) from aboral ectodermal cells. The SOM, which is composed of proteins, saccharides, and lipids, performs functions critical for skeleton formation. Even though polysaccharides constitute the major component of the SOM, its contribution to coral skeleton formation is poorly understood. To this end, we analyzed the SOM of the massive colonial coral, *Porites australiensis*, the skeleton of which has drawn great research interest because it records environmental conditions throughout the life of the colony. The coral skeleton was extensively cleaned, decalcified with acetic acid, and organic fractions were separated based on solubility. These fractions were analyzed using various techniques, including SDS-PAGE, FT-IR, *in vitro* crystallization, CHNS analysis, chromatography analysis of monosaccharide and enzyme-linked lectin assay (ELLA). We confirmed the acidic nature of SOM and the presence of sulphate, which is thought to initiate $CaCO_3$ crystallization. In order to analyze glycan structures, we performed ELLA on the soluble SOM for the first time and found that it exhibits strong specificity to *Datura stramonium* lectin (DSL). Furthermore, using biotinylated DSL with anti-biotin antibody conjugated to nanogold, *in situ* localization of DSL-binding polysaccharides in the *P. australiensis* skeleton was performed. Signals were distributed on the surfaces of fiber-like crystals of the skeleton, suggesting that polysaccharides may modulate crystal shape. Our study emphasizes the importance of sugar moieties in biomineralization of scleractinian corals.

Keywords

Porites australiensis, biomineralization, coral, skeletal organic matrix, saccharide

Abbreviations

AIM: acid-insoluble matrix

ASM: acid-soluble matrix

DSL: *Datura stramonium* lectin

ELLA: enzyme-linked lectin assay

FT-IR: Fourier transform infrared spectroscopy

SOM: skeletal organic matrix

Introduction

Scleractinian corals are marine animals known for their capacity to elaborate calcium carbonate exoskeletons of complex shapes, many of which form reefs of great size (Spalding et al., 2001). Among metazoans, scleractinians are the main producers of biogenic aragonite in marine ecosystems (Milliman, 1993). From a geochemical viewpoint, scleractinian biomineralization can be considered as the uptake of inorganic ions from the environment and conversion of these ions into a spatially structured network of calcium carbonate biocrystals that contain trace elements (Beck et al., 1992; Tambutté et al., 2011). Because this process literally 'freezes' environmental information into skeletal tissues that fuel steadily sedimentary archives, scleractinian skeletons are often used to reconstruct sequences of paleoenvironmental conditions, in particular, past seawater temperatures via measures of Sr/Ca, Li/Ca, and $\delta^{18}O/\ \delta^{16}O$ ratios (Beck et al., 1992; Druffel, 1997; Hathorne et al., 2013; Simkiss and Wilbur, 2012) or past ocean pH via boron isotopic composition ($\delta^{11}B$) (Rollion-Bard et al., 2011). However, in spite of the increasing use of these geochemical proxies in corals, the molecular basis of scleractinian skeleton formation is far from understood.

From a cellular viewpoint, scleractinian skeletal biomineralization is typically an epithelium-driven process, *i.e.,* all precursor components of the exoskeleton are secreted by the calicoblastic epithelium (also called the aboral ectoderm), a subset of the ectoderm (Allemand et al., 2004; Constantz and Weiner, 1988; Tambutté et al., 2011), in contact with the nascent mineral layer. These components comprise inorganic ions - calcium, bicarbonate and minor elements, *i.e.*, strontium and magnesium - that are extruded via membrane channels and pumps (transcellular pathway) or via intercellular space (paracellular pathway), and are combined into $CaCO_3$ minerals in the sub-calicoblastic space (Tambutté et al., 2011). They also include a large set of organic macromolecules that constitute the skeletal organic matrix (SOM), which is allegedly released via a classical secretory pathway. This latter is however poorly documented for cnidarians in general.

From a biochemical viewpoint, in many coral species examined to date, the SOM contains proteins, glycoproteins, lipids, and polysaccharides that are included in the skeleton during the calcification process (Constantz and Weiner, 1988; Cuif et al., 1999b; Dauphin, 2001; Farre et al., 2010; Puverel et al., 2005). The SOM is distributed heterogeneously in the coral skeleton, being concentrated in "centres of crystallization" (Bryan, 1941; Ogilvie, 1896) or in "early

mineralization zones" (Cuif et al., 2003), from which fiber-like crystals distribute radially. The SOM is also detected on the top surface and growing steps in crystals (Cuif and Dauphin, 2005). The complex topographical relationship between the organic and mineral phases suggests that the SOM plays an active role in regulating the initiation and growth of the calcium carbonate crystals. In particular, the SOM contains acidic macromolecules, usually considered as key-components for interacting with calcium carbonate crystals: in different *in vitro* functional assays, they have been shown to bind calcium ions (Isa and Okazaki, 1987) and modify the shapes of calcium carbonate crystal (Naggi et al., 2018; Ramos-Silva et al., 2014) similarly to what has been observed with mollusc SOM (Addadi and Weiner, 1985; Weiner and Hood, 1975). Amino acid analyses of SOMs of various coral species reported high contents of aspartic and glutamic acids (Constantz and Weiner, 1988; Cuif et al., 1999a; Gautret et al., 1997; Mitterer, 1978; Puverel et al., 2005). More recently, aspartic acid-rich proteins in coral skeletons were predicted by whole genome sequencing of *Acropora digitifera* (Shinzato et al., 2011), and subsequently confirmed by transcriptomic and proteomic studies (Drake et al., 2013; Ramos-Silva et al., 2013b; Takeuchi et al., 2016).

Contrary to these recent comprehensive surveys of skeletal proteomes, sugar moieties in coral SOM have not been well characterized, even though they are always detected in coral skeletons and are believed to play important, although undetermined functions in biomineralization (Albeck et al., 1996). The sugars in coral SOM include common monosaccharides, such as neutral (fucose, rhamnose, galactose, glucose, mannose, xylose), aminated (galactosamine and glucosamine) and acidic (glucuronic/galacturonic acids) hexoses. Previous studies showed that their proportions vary greatly among species (Cuif et al., 1999b; Naggi et al., 2018; Ramos-Silva et al., 2014), such that some present remarkable monosaccharide signatures. For example, in the *Acropora millepora* SOM, arabinose represents more than 60% of all monosaccharides, a finding correlated with its abundance in mucus of that species (Ramos-Silva et al., 2014; Wild et al., 2005). In addition, sulphated acidic sugars were detected in SOMs of several scleractinian coral species (Dauphin et al., 2008; Puverel et al., 2005). However, polymeric structure and localization of saccharides in coral skeletons have not been studied.

In this context, we have undertaken the overall biochemical characterization of the SOM of the massive colonial coral, *Porites australiensis*. By virtue of their longevity and ability to accumulate massive calcium carbonate skeletons, the genus *Porites* represents one of the most

important corals as a recorder of environmental conditions (Beck et al., 1992; Cobb et al., 2003; Linsley et al., 2000; Watanabe et al., 2011). We characterized the *Porites* SOM by using various molecular analyses, including SDS-PAGE, FT-IR, CHNS analysis, and *in vitro* calcium carbonate crystallization experiment. We confirmed the presence of sulphate, which contributes to the acidic nature of the *Porites* SOM. Furthermore, monosaccharides were quantified, and for the first time in corals, enzyme-linked lectin assay (ELLA) was performed. *In situ* localization of polysaccharide in coral skeleton was achieved using a biotinylated lectin (*Datura stramonium* Lectin - DSL) associated with anti-biotin antibody conjugated to nanogold. Our results showed that a DSL-reactive saccharide fraction was evenly dispersed on the surfaces of calcium carbonate crystals, suggesting that it may shape crystal growth during coral skeleton formation.

Materials and methods

Sample collection and cleaning

A living coral colony of *Porites australiensis* (approx. weight 50 grams) was collected at the Sesoko Marine Station, University of Ryukyus, Okinawa, Japan, under Okinawa prefecture permit (Number: 20–69). The organism was immersed overnight in 3L of 10x diluted household bleach solution and then extensively rinsed with water. This process, which was continued until the complete removal of animal tissue and other organisms on the surface, comprised the initial bleaching. The coral skeleton was rinsed, air-dried, and crushed into ~2mm fragments with a Jaw-crusher (Retsch BB200). Fragments were immersed in 0.1x sodium hypochlorite 10-15% (SIGMA ref. number 71696) for 50h (second bleaching). Then, the fragments were washed with twice-distilled water, dried, and powdered using a mortar grinder (Frisch Pulverisette 2). The powder (48 grams) was sieved (pore size <200 µm) and separated into two batches. The first was subsequently decalcified (see below), while the second was bleached overnight in NaOCl solution (third bleaching), thoroughly washed and air-dried at 37°C before decalcification.

Extraction of skeletal organic matrices

The cleaned powder samples (second or third bleaching) were suspended in cold water and decalcified overnight at 4°C by progressively adding (100 µL every 5 sec.) cold dilute acetic acid (10% vol/vol) with an electronic burette (Titronic Universal, Schott, Mainz, Germany).

After 15 hours (final pH 4), the clear solution was centrifuged (3900 G, 30 min.), in order to separate the pellet containing the acid-insoluble matrix or AIM from the supernatant, *i.e.*, the acid-soluble matrix (ASM). The AIM pellet was resuspended in Milli-Q water, centrifuged, and the supernatant discarded. After three cycles, the pellet was freeze-dried. The ASM solution was filtered (5 µm) on a Nalgene filtration apparatus and concentrated by ultrafiltration (Amicon stirred cell 400 mL) on a 10kDa cutoff membrane (Millipore, ref. PLGC07610). The concentrated solution (15 mL) was dialyzed 4 days against 1 L MilliQ water with several water changes, and freeze-dried.

SDS-PAGE

ASM lyophilisates were suspended in Milli-Q and an aliquot was added to an equal volume of 2x Laemmli sample buffer containing ß-mercaptoethanol. AIM pellets were gently fragmented with a scalpel and a part was directly resuspended in 1x Laemmli sample buffer. All preparations were denatured for 5 min at 99˚C, cooled on ice and briefly centrifuged. While ASM was totally dissolved by denaturation, a part of AIM remained insoluble. Consequently, only the Laemmli-soluble fraction of AIM (referred to as LS-AIM) was further analyzed on gels. Proteins were run on precast 10%-20% gradient mini-gels (Bio-Rad) in mini-Protean III system. Gels were stained with silver nitrate (Morrissey, 1981), Stains-all (Campbell et al., 1983; Marin et al., 2005) and Alcian blue (Thornton et al., 1996) at pH 1.0 in order to detect sulphate groups.

FT-IR spectroscopy

FT-IR spectroscopy was used to check the overall chemical properties of the extracted matrices (ASM and AIM) after two or three bleaching steps. In each case, minute chips of lyophilized samples were analyzed with a Bruker Vector 22 instrument (Bruker Optics Sarl, Marne la Vallée, France) fitted with a Specac Golden Gate Attenuated Total reflectance (ATR) device (Specac Ltd, Orpington, UK) in the 4000–500 cm^{-1} wavenumber range (twelve scans at a spectral resolution of 4 cm^{-1}). The choice for ATR mode was dictated by its reliability and reproducibility, as recently shown (Beasley et al., 2014). The qualitative assignment of absorption bands was performed by comparison with previously described spectra, determined by us or available in the literature (Dauphin, 2001; Dauphin et al., 2008; Kanold et al., 2015).

Elemental analysis

Elemental analyses were performed at the ‘‘Plateforme d’Analyse Chimique et de Synthèse Moléculaire de l’Université de Bourgogne (PACSMUB)’’ on a Fisons EA 1108 CHNS-O apparatus (M. Soustelle). As the technique requires 5 mg of material, only one AIM extract (AIM 3bl) was tested, and the measurement was performed twice.

In vitro crystallization of $CaCO_3$ with ASM

In vitro crystal growth experiments in the presence of ASM was tested as described in a previous paper (Kanold et al., 2015). In brief, 200 µL of 10 mM $CaCl_2$ containing ASM at increasing concentrations (1-32 µg/ml) was applied to a 16-well culture slide (Lab-Tek, Nunc/Thermo Scientific, Rochester, NY, USA). The glass slide was closed with a plastic cover in which 1-mm holes were pierced above each well to allow exposure of the solution to ammonium bicarbonate vapor, and sealed with Parafilm. The slide was placed in a desiccator, together with ammonium bicarbonate crystals, under vacuum and incubated at 4 ˚C for 3 days. Subsequently, the solution was carefully removed by suction with a blunt needle connected to a vacuum pump and $CaCO_3$ crystals generated on the glass bottom were dried for 4h at 37˚C. These were directly observed using a tabletop scanning electron microscope (TM 1000, Hitachi) without carbon sputtering.

Monosaccharide analysis

Monosaccharide quantification of ASMs and AIMs after two or three bleaching steps was performed according to the HPAE-PAD technology (High Pressure Anion-Exchange - Pulsed Amperometric Detection) on an ICS-3000, Dionex system equipped with a Dionex CarboPac™ PA-20 (3x150 mm) analytical column. In short, lyophilized samples were hydrolyzed in 2M trifluoroacetic acid at 105 °C for 4 h (100 µg/100 µL), and the solution was neutralized with sodium hydroxide. Hydrolytic conditions deacetylate N-acetyl-glucosamine and N-acetyl-galactosamine, which are subsequently analyzed as glucosamine and galactosamine, respectively. Filtered samples (20 µL) were eluted at 0.4 mL/min (35°C) using the following sodium hydroxide gradient: pure water 99.2% /250 mM NaOH 0.8% : 0→20 min; pure water 75%/250 mM NaOH 20% /NaOAc (1M)- NaOH (20 mM) 5%: 20→37min ; pure water 40% /250 mM NaOH 20%/NaOAc (1M)-NaOH (20 mM) 40%: 37→41min. Each elution was followed by a wash and subsequent equilibration time. External sugar and uronic acids standards were used for calibration (7 points per curve): fucose, glucose, xylose, galactose, mannose, rhamnose, arabinose, glucosamine, galactosamine, galacturonic acid and glucuronic acid (all provided by Sigma-Aldrich).

Enzyme-Linked Lectin Assay (ELLA)

Enzyme Linked Lectin Assay (ELLA) was conducted as described previously (Kanold et al., 2015) on ASM fractions. This test, performed in solution, cannot be applied to AIM. Briefly, 96-well plates (MaxiSorp, Nunc/Thermo Scientific, Nunc A/S, Roskilde, Denmark) were coated with ASM (50 ng/well) and incubated for 90 min at 37˚C. They were washed three times with a solution of TBS/Tween-20 (0.5 mL Tween 20 per L) spread using a manual microplate 8-channel washer (Nunc Immuno Wash), and subsequently blocked with Carbo-free blocking solution (Vector Laboratories, ref. SP-5040) for 60 min at 37˚C. Three sets of 7 biotinylated lectins were tested (Vector Laboratories, Peterborough, UK, ref. BK-1000, BK-2000, BK-3000). They were applied to the wells (dilution to 10 µg/mL) and incubated for 90 min at 37˚C. Unbound lectins were removed by washing five times with TBS/Tween-20. Then, a solution containing alkaline phosphatase-conjugated avidin (Avidin-AP, Sigma A7294, St Louis, MO, USA) diluted 70,000 times was added (100 µL per well) and incubated for 90 min at 37 ˚C. Microplates were washed as before, and incubated with ELISA substrate solution (10% vol/vol diethanolamine in Milli-Q water, pH 9.8) containing phosphatase substrate (0.5 mg/mL, 4-nitrophenyl phosphate disodium salt hexahydrate (pNPP) tablet, Sigma, ref. UN3500-A) at 37 °C. They were incubated at 37°C and read every 15 minutes at 405 nm using a Bio-Rad Model 680 micro-plate reader. Results were normalized and converted to percentage of reactivity by subtracting the background (negative control comprising ASM without lectin but with Avidin-AP) from all values and by considering the highest response as 100%. The test was repeated at least three times. For detailed information on the binding preference of each lectin, see Immel et al. (Immel et al., 2016).

***In situ* localization: lectin-gold assay.**

Sodium hypochlorite-bleached fragments of *P. australiensis* skeleton were cut with a diamond saw (Dremel) and one surface was flattened with fine sand paper. After rinsing with sonication, the surface was finely polished with an alumine suspension (0.05 µm) on a rotary polisher until a mirror polish was obtained. Samples were thoroughly cleaned by sonication and submitted to bleach (NaOCl, 0.26 % active chlorine) to remove contaminants that may have spread over the surface during polishing. They were rinsed twice with Milli-Q water, and gently dried on Whatman paper. The flat surface was then etched 5 minutes with a solution of 1% EDTA (wt/vol) in the sonication bath to expose the skeletal matrix, then rinsed with Milli-Q water (5 min.).

All incubation steps described after were performed at room temperature. In brief, coral samples were incubated one hour in Carbo-free blocking solution alone ((Vector Laboratories, ref. SP-5040), then overnight in the same solution containing the biotinylated DSL (*Datura stramonium* lectin, diluted 100 times), and in the presence of the bactericidal agent, sodium azide (0.005% wt/vol). Samples were gently rinsed several times with TBS/Tween20, then incubated at least 90 minutes in a Carbo-free solution containing diluted (1/100) goat anti-biotin antibody conjugated to ultra-small gold particles (0.8 nm) (GABio, Ultra Small, ref. 800.088; Aurion, Wareningen, The Netherlands). Samples were rinsed several times with TBS/tween20 and gently dried on filter paper. Enhancement of the gold signal was achieved by incubating samples in silver enhancement solution (British Biocell International, ref. SEKL15) for about 15-20 minutes. Samples were rinsed once in Milli-Q water, then dried at 37°C.

Negative controls were performed in parallel under identical conditions, by omitting one or more incubation steps: no incubation step with DSL; incubation with gold-coupled anti-biotin, followed by silver enhancement; no incubation with DSL nor with biotin, but with silver enhancement. All samples were carbon-sputtered and observed either with a JEOL JSM 760 F field emission scanning electron microscope (JEOL, Tokyo, Japan) or with an ultra-high resolution, cold-field emission Hitachi SU8230 scanning electron microscope. Quick checks were performed with a tabletop SEM Hitachi TM1000. The experiment was repeated five times.

Results

Cleaning of coral skeleton and total matrix quantification

Because the *Porites* skeleton is porous, having a mesh-like structure, thorough cleaning of the skeleton was required to remove soft tissues of the coral and microorganisms present in the pores. We repeatedly cleaned pieces of coral skeleton by immersing them completely in bleach solution and rinsing exhaustively with ultrapure water until tissue and epibionts on the skeletal surface were completely removed (first bleaching). However, even though the skeleton looked superficially clean after this initial treatment, a careful check using SEM indicated that fibrous organic material was still present in the pores (Figure 1A, C). After a

second bleach treatment, these contaminants were removed (Figure 1B, D). Finally, to ensure the complete removal of contaminants, a third bleaching was performed on sieved skeletal powder (grain size < 200 µm). The total organic matrices were quantified after 2nd and 3rd bleaching as shown in Table 1. Interestingly, the amount of organic matrix - both soluble (ASM) and insoluble (AIM) - extracted after the 3rd bleaching was significantly lower (reduced by half) than that obtained after the 2nd one. The organic matrix represents 0.14% and 0.07% of the total skeleton by weight, after the 2nd and the 3rd bleaching, respectively.

SDS-PAGE

The ASM and the AIM (or, at least, its Laemmli-soluble moieties, referred to as LS-AIM) extracted from the 2nd and 3rd bleachings were analyzed by poly-acrylamide gel electrophoresis (SDS-PAGE) after staining with silver nitrate, Stains-all, and Alcian blue (Figure 2). Overall, broad and smeary staining was observed in all staining methods. Weak, blurred bands of high molecular weight (>170 kDa) and in the range of 50-70 kDa were detected in the silver stained gel, as well as negatively stained zones at the bottom of the lanes (<10 kDa for lane 2nd bleaching, and <17 kDa for the three other lanes) (Figure 2A). Stains-all staining showed a strong purple color in ASMs, while AIMs appeared more pinkish. (Figure 2B). Such purple staining - between metachromatic blue and red - has already been observed in a previous study for ASM of other skeletal matrices, suggesting their ability to bind calcium (Marin et al., 2005). Alcian blue staining at low-pH (pH 1.0) stained both ASM and AIM (Figure 2C), suggesting the presence of sulphate groups in all four samples (Thornton et al., 1996). Low-molecular weight ASMs stained more intensely, while for AIMS, high-molecular weight compounds stained more strongly.

FT-IR and CHNS analyses

Fourier transform infrared (FT-IR) spectra were analyzed for SOMs (Figure 3). First, the absence of the typical carbonate peaks in the ASM and in the AIM demonstrated that both extracts did not contain any contaminating salts resulting from the decalcification. In all fractions, bands attributed to protein or sugar backbones were detected at around 3380 cm^{-1}, 1650 cm^{-1}, and 1540 cm^{-1}, which correspond to amide A (νN-H), amide I (νC=O), and amide II (νC-N) bands, respectively. The signal of amide I band was stronger than that of amide II in ASM samples, while they were equivalent in AIM fractions. Weak signals at 2921-2923 cm^{-1} in AIM and 2927-2937 cm^{-1} in ASM, representing νC-H stretching vibrations, were also detected and may correspond to lipids. Signals around 1450 and 1410 cm^{-1} may be related to

carboxylic groups. An absorption band specific to carbohydrate was observed near 1060-1070 cm^{-1} in all samples. In AIM fractions, this signal was significantly weaker after the third bleaching AIM with respect to the adjacent signal at 1150 cm^{-1}, which was sharply detected in both AIM samples. The band at 1150 cm^{-1}, together with signals at 961, 636 and 554 cm^{-1}, corresponds to phosphate group (Panda et al., 2003; Rivera-Muñoz, 2011). These bands were hardly visible in ASM (shoulders at 1150 cm^{-1} and 961 cm^{-1}); presumably because of their weak amplitudes, they were masked by other broad signals. The signal at 1230-1250 cm^{-1} is related to νS=O stretching vibration (Cabassi et al., 1978; Cael et al., 1976; Longas and Breitweiser, 1991). The presence of sulfur in the third bleaching AIM was also supported by CHNS analysis (Table 2).

***In vitro* $CaCO_3$ crystallization with ASM**

Results of the *in vitro* crystallization assay (diffusion test) are shown in Figure 4. Crystals were grown in solution containing ASM, extracted after two (Figure 4A to E) and three (Figure 4G to L) bleach treatments. Addition of 1 µg/mL ASM (Figure 4A, G) resulted in almost no difference with the control experiment (without ASM, Figure 4M), in which typical, rhombohedral calcite crystals were synthesized. The morphology of crystals was altered in the presence of 4 µg/mL ASM (Figure 4B, H). Terraced structure appeared on the edges, and the crystal size was reduced. The increased concentration of ASM (16 µg/mL, 2nd bleach) resulted in polycrystalline structure (Figure 4C, D), and this effect was more significant at 32 µg/mL of ASM (Figure E, F). In comparison, the alteration of crystal shape was more severe when high concentrations of ASM extracted after 3 bleaching steps were used: at 16 µg/mL, crystal edges were rounded and the surface was rough-textured (Figure 4I, J). At the highest concentration (32 µg/mL), flat crystal faces were completely destroyed, and aggregation of crystals was frequently observed (Figure 4K, L). In summary, higher concentrations of ASMs altered the morphology and size of $CaCO_3$ crystals, and this effect was more accentuated when using ASM extracted after 3 bleaching steps.

Monosaccharide analysis

Results of the monosaccharide analysis after mild hydrolysis (with TFA) of both ASM and AIM, after 2 or 3 bleaching steps, are shown in Figure 5, as relative percentages of the total sugar composition. The data allow a double comparison, between AIM and ASM on the one hand, and between the 2nd and 3rd bleaching on the other hand. First, in both ASMs, the most abundant saccharides are galactose>arabinose>fucose, with the two first representing ≥50%

of all sugars. Xylose, glucosamine, glucose and mannose are minor monosaccharides (between 4 and 10%) while rhamnose and galactosamine are quantitatively negligible (below 3%). The sugar profiles of both AIMs are somewhat similar to those of ASMs, except that galactose and glucose are the dominant sugars (~≥ 20% each), with ~15% arabinose. Xylose and fucose (>10%) are next most abundant, followed by glucosamine and mannose (5-10%). As in ASMs, rhamnose and galactosamine are extremely minor. Galacturonic and glucuronic acids were not detected in any of our samples. Second, the third bleaching treatment had a more pronounced effect on ASMs than on AIMs: while it did not modify the sugar abundances in AIMs, resulting in two superimposable AIM histogram patterns, it induced in ASM a large decrease of arabinose (from 36.2 to 20.7%) and slight increases in galactose (28.6 to 29.2%), fucose (13.2 to 16.2%), glucosamine (4.2 to 8.4%), glucose (5.1 to 7.4%) and xylose (5.6 to 8.6%). However, in spite of these few percentage changes, the 3rd bleaching did not fundamentally modify the monosaccharide composition pattern of ASM.

ELLA

In order to determine the types of glycan structures present in ASM (extracted after two and three bleaching steps), the affinity of these two extracts for biotinylated lectins was examined by enzyme-linked lectin assay (ELLA) (Kanold et al., 2015). The results, expressed as percentages of reactivity with respect to the most reactive lectin, are shown in Figure 6. It is noteworthy that the two ASM extracts reacted almost identically to the 21 different lectins: in both cases, the strongest signal by far was observed with *Datura stramonium* lectin (DSL), which preferentially binds to (β-1,4) linked GlcNAc oligomers, LacNAc, and poly-LacNAc (Sondej et al., 2009). Greatly reduced affinities (20-25% of those obtained with DSL) were recorded with Concanavalin A (ConA), *Lycopersicon esculentum* lectin (LEL), and *Solanum tuberosum* lectin (STL). Other lectins including, SBA, DBA, PSA, LCA, RCA_{120}, PHA-E, ECL, UEA I, SJA, PNA, Jacalin, WGA, GSL I, PHA-L, Succinylated WGA, VVA, and GSL II, exhibited very weak reactivity (less than 15% of DSL) for the two ASM extracts.

***In situ* localization study using gold-conjugated DSL**

Since DSL showed the strongest affinity to *Porites* ASM in ELLA, an *in situ* assay was developed to localize the target saccharide moiety in the coral skeleton. Figure 7 shows SEM images of the coral skeleton treated with biotinylated DSL, which was subsequently targeted with an anti-biotin antibody coupled with gold nanoparticles. Figure 7A, acquired in secondary electron (SE) mode, shows tips of the fibers that radiate from the early

mineralization zone (not shown), where crystallization occurs. Figure 7B presents the same area in back-scattered electron (BSE) mode. It shows tiny bright spots that represent gold particles, and consequently sugar-bound biotinylated lectins. Since an SEM image in SE mode (Figure 7A) does not show any signal, this confirms that the signals detected in BSE mode come from the gold particles. In Figure 7B, there is no particular concentration of gold signals at the apex of the fibers, as one might have expected. Rather, the signals are dispersed along the crystal surfaces.

Figures 7C, D and E (in BSE mode) display successive enlargements of the same area. Here again, one notices that signals are homogeneously distributed on the surfaces of the fibers, irrespective of the growth lines (belt-like structures) that are perpendicular to the direction of crystal growth (Figure 7C and D). At high magnification (Figure 7E), the density of spots reaches about 10-15 per μm^2. At very high magnification (x100 000), gold particles can be measured (diameter ~ 50 nm) (Figure 7F). In none of our experiments did we detect concentrations of gold spots near the centers of the spherulites, a finding that may suggest that DSL-binding sugar moieties are not involved in crystal nucleation, but that they have other functions related to crystal growth. Negative controls are shown on Figure 7G (SE mode) and H (BSE mode). Very few signals were obtained when gold-coupled anti-biotin was added to the skeleton in the absence of biotinylated DLS, confirming the low background of the sample and the specificity of sugar labeling.

Discussion

In the present study, we have characterized the skeletal organic matrix (SOM) of the massive coral, *Porites australiensis,* using various biochemical techniques, including FT-IR, CHNS, ELLA, gel electrophoresis, monosaccharide analysis by chromatography, and *in vitro* crystallization. We have also localized sugar components directly in the coral skeleton, with a technique that we adapted for the first time for corals. Our discussion focuses on three points: the influence of the bleaching, the presence of sulphate and the properties of the sugar moieties.

As discussed in one of our earlier papers (Ramos-Silva et al., 2013a), bleaching coral skeletal tissues with sodium hypochlorite is crucial for obtaining a SOM free of organic contaminants, namely soft tissues originating from the ectoderm, or microorganisms accumulated in skeletal pores and pockets. We chose a cleaning strategy consisting of successive bleaching treatments

to eliminate these contaminants, and characterized the extracted SOMs (ASMs, AIMs) after the second and third bleaching steps. Depending on the technique used, we found either that the third bleaching did not produce any modification of the biochemical properties of the SOMs, or that it induced some significant changes.

Among the techniques that did not detect any change, SDS-PAGE, regardless of the staining used, showed smeared patterns in all SOMs, with no differences between the two ASMs and the two AIMs. Similarly, ELLA on the two ASMs showed that both exhibit very similar lectin-binding signatures featuring strong reactivity with DSL, moderate affinity with ConA and LEL, and very low affinity with all 18 other lectins. Last, monosaccharide analyses of the AIMs showed almost no differences in their composition. Taken together, these techniques suggest that the third bleaching did not alter the qualitative biochemical characteristics of the saccharidic moieties of the SOM.

However, other techniques employed in our study evidenced noticeable effects that were induced by the third bleaching step. First, the SOM quantity (ASM and AIM) was reduced by half. Second, FT-IR detected a decrease of the sugar peak around 1000-1050 cm^{-1} for both ASM and AIM. Third, monosaccharide analysis of the ASMs showed that arabinose was significantly reduced. Finally, the *in vitro* crystallization assay evidenced a noticeable difference: the ASM extracted after the third bleaching induced stronger effects on crystal morphologies than the ASM extracted after the second bleaching. These results suggest that some sugar-containing macromolecules of the SOM (either polysaccharides or glycoproteins) are peripheral to the mineral grains and destroyed by the third bleaching step, while some others are protected from the harsh treatment and should be considered as 'intracrystalline', to employ the old terminology of Crenshaw (Crenshaw, 1972). It is significant that the 'intracrystalline' ASM fraction, which is supposed to have a strong affinity for calcium carbonate, induces stronger effects *in vitro* than the ASM extracted after two bleaching steps. To summarize this point, we reemphasize the importance of cleaning skeletal tissues with sodium hypochlorite and think that applying successive bleaching steps to the skeletal powder may be an elegant manner to pre-select SOM macromolecules that have the highest affinity to the mineral phase.

Our second focus is the presence of sulphate in the SOM of *Porites australiensis*, demonstrated by Alcian blue staining at low pH, FT-IR, and CHNS analysis. First, Alcian blue binds polyanionic groups, whatever they are, in particular those found in mucopolysaccharides. At low pH (=1), Alcian blue specifically binds sulphate-containing

466 mucopolysaccharides (Thornton et al., 1996). In the present case, both ASM and LS-AIM are
467 stained, but not identically: stronger staining occurred in the lower two-thirds of the gel for
468 ASM, and the upper third for LS-AIM, indicating that the distribution of sulphate differs in
469 these two fractions. Bulk analysis by FT-IR spectroscopy confirms the presence of sulphate
470 groups, characterized by a peak in the range 1200-1250 cm^{-1}. Interestingly, pairwise
471 comparisons of sulphate peak amplitudes from the second and third bleaching steps showed
472 that the additional cleaning treatment did not degrade sulphate. This result is consistent with
473 the CHNS analysis, which unambiguously detected sulfur (>1%) in AIM after three bleaching
474 steps. Our data consequently suggest that the sulphate-containing macromolecules - likely
475 polysaccharides - are truly intracrystalline.
476 More generally, the presence of sulfur in coral skeletons is a recurrent finding that leaves the
477 question of its role open (Dauphin et al., 2008). Previous studies demonstrated that sulfur was
478 present in the SOM of *Stylophora*, *Pavona*, *Hydnophora*, and *Merulina* (Dauphin et al., 2008;
479 Puverel et al., 2005). Furthermore, sulphated sugars were found to be predominant over
480 sulfur-containing amino acids (methionine and cysteine) in ASM (Dauphin et al., 2008). As a
481 general rule, sulphated groups on sugars (ester sulphate) increase the acidic nature of the
482 SOM. They can bind calcium ions or exert an ionotropic effect by creating a very localized
483 anionic environment to concentrate calcium ions in the vicinity of the nucleation spots.
484 Sulphate is concentrated in early mineralization zones, suggesting that it may also promote
485 crystal formation (Cuif et al., 2003; Lloyd et al., 1961). Interestingly, in other calcified tissues,
486 such as nacre of the cephalopod *Nautilus pompilius*, a chemical mapping of single nacre
487 tablets showed that sulphate-containing macromolecules were localized in a central annular
488 zone in close association with carboxylate-rich macromolecules that are supposed to be the
489 calcium carbonate nucleators (Nudelman et al., 2006). This peculiar localization suggests a
490 cooperative role of both categories of macromolecules. Clearly, future work on coral
491 biomineralization should elucidate the precise function of sulphated sugars, either as Ca^{2+}
492 concentrators or as mineral nucleators.
493
494 The third focus of our discussion concerns some specific properties of the saccharidic
495 moieties of *Porites australiensis* SOM, including the lectin-binding signature, the
496 monosaccharide composition and the *in situ* localization of DSL-binding saccharide. At first,
497 the peculiar lectin-binding signature of the ASM deserves mention. Among all tested lectins,
498 DSL gave by far the strongest signal. DSL, a lectin extracted from the jimson weed, binds
499 chitotriose, chitobiose, and N-acetyl-D-glucosamine, with decreasing affinity. Its

carbohydrate-binding site recognizes oligomers of N-acetyl-D-glucosamine; thus, it exhibits strong affinity for chitin. DSL also binds the disaccharide N-acetyllactosamine (formed from the condensation of beta-galactose and N-acetyl-glucosamine) and its oligomers. It is remarkable that other lectins that typically bind chitin / chitin-like motifs, such as WGA, STL, or LEL give very little or no signal with the ASM of *P. australiensis.* This may suggest that the saccharidic motif predominant in ASM is not N-acetyl-glucosamine, but rather N-acetyllactosamine or its oligomers. This is consistent with the high amount of galactose, by far the most abundant monosaccharide identified in ASM and AIM. On the other hand, none of the galactose-binding lectins, such as jacalin, PNA, SBA, GSL-1, RCA, and SJA give signal with *P. australiensis* ASM, but their lack of reactivity may reflect individual recognition specificities for each of them, as listed by Immel and coworkers (Immel et al., 2016). Beside this, additional useful structural information can be extracted from lectin signature: for instance, jacalin interacts with most O-linked glycoproteins, but is unreactive with ASM, while ConA, a lectin that binds mannose of N-linked glycopeptides, gives the second highest signal (although moderate). This may suggest that most ASM glycoproteins of *P. australiensis* skeleton are of the N-linked-type. Fucose is the third most abundant monosaccharide in ASM, but UEA-1, which binds strongly to α(1,2)-linked fucose, does not react. This suggests either that fucose residues present in the ASM are predominantly of the α(1,3) or α(1,6)-types, or that they occupy internal positions in the saccharidic chains, or that they form fucose-containing trisaccharides, a motif that inhibits UEA-1.

Finally, the three most abundant sugar residues of *P. australiensis* ASM, namely galactose, arabinose, and fucose, represent the residues that are predominantly represented in the soluble SOM of two acroporid corals, *Montipora caliculata* and *Astreopora myriophtalma* (Cuif et al., 1996). Galactose and fucose are also abundant in *Heliastrea curta* and *Fungia rependa* while galactose and arabinose predominate in *Acropora danae* (Cuif et al., 1996). Interestingly, the monosaccharide composition of *P. australiensis* ASM is in agreement with that of zooxanthellate coral ASMs in general, which was statistically distinguished from that of non-zooxanthellate coral ASMs by the presence of arabinose - a monosaccharide exclusive to zooxanthellate corals - the abundance of galactose, and low amounts of galactosamine and glucosamine (Cuif et al., 1999b). This monosaccharide composition contrasts singularly with that recently published by Naggi and coworkers (2018) who identified by other techniques (chromatography and mass spectrometry) glucuronic acid as the main saccharide residue present in the SOM of three stony corals, *Astroides calycularis*, *Balanophyllia europaea*, and *Stylophora pistillata*. We did not detect this acidic sugar in our samples and then reason of the

discrepancy between our data and theirs is not known.

Last, using gold-conjugated DSL, we localized sugar components that have a strong affinity to DSL lectin. In all experiments, we obtained a homogeneous distribution of gold particles on the surface of radiating aragonite fibers. We did not observe signals concentrated along growth lines, perpendicular to fiber elongation nor signals at the tips of the fibers. Finally, the centers of spherulites are enriched in organics that are supposed to be the nucleating macromolecules. However, we did not detect any high concentration of gold spots around these centers, *i.e.,* at the bases of the fibers that are the closest to the center. In this latter case, we cannot exclude that the treatment of the polished surface - prior to lectin incubation - which consists in cleaning with bleach followed by slight etching with EDTA, may have eliminated most of the organics located at the centers of spherulites. In spite of these potential preparation artifacts, our observations suggest that the DSL-binding saccharide fraction is neither involved in crystal nucleation nor in stopping crystal growth (where it would be distributed along the growth lines). Because the signal homogeneously covers the aragonite fibers, and because DSL-reactive ASM exerts a significant *in vitro* effect on crystal size and shape, we put forward the hypothesis that this fraction modulates size, shape, and/or fiber growth kinetics. In order to better understand the role of these sugar moieties in *P. australiensis* biomineralization, further experiments, such as *in vitro* crystallization experiments with purified DSL-binding polysaccharide, should be conducted.

Conclusions

Our study represents the first biochemical characterization of the skeletal organic matrix of the massive coral, *Porites australiensis*, under different cleaning conditions. We focused on the sugar moieties. Besides obtaining peculiar signatures of monosaccharide composition and of lectin profile, we localized *in situ*, for the first time, a DSL lectin-binding fraction. Our results re-emphasize the role of saccharides in coral biomineralization and aims at identifying sugar signatures of coral SOMs, by waiting for understanding the structure-function relationships of this class of macromolecules in biomineralization. Further investigation of this organic fraction, together with the ongoing proteomic analysis of *Porites* SOM, is essential to obtain the most complete picture of macromolecular constituents required for building the skeleton of these major reef-forming corals.

567

Acknowledgements

We thank Dr. Akira Iguchi (Okinawa National College of Technology) for providing coral specimens. We also thank Marcel Soustelle (PACSMUB, Dijon) for elemental analysis and Frédéric Herbst for helping in handling the two SEM. We thank Dr. Steven D. Aird for editing the manuscript. All data were generated during a six-month stay of Dr. T. Takeuchi (Oct. 2015-March 2016) in the laboratory of Dr. F. Marin, UMR CNRS 6282 Biogéosciences in Dijon (UBFC).

Funding

This study was supported by internal funds from the Okinawa Institute of Science and Technology (OIST).

References

Addadi, L., Weiner, S., 1985. Interactions between acidic proteins and crystals: stereochemical requirements in biomineralization. Proc. Natl. Acad. Sci. U. S. A. 82, 4110-4114.

Albeck, S., Weiner, S., Addadi, L., 1996. Polysaccharides of Intracrystalline Glycoproteins Modulate Calcite Crystal Growth In Vitro. Chemistry – A European Journal 2, 278-284.

Allemand, D., Ferrier-Pagès, C., Furla, P., Houlbrèque, F., Puverel, S., Reynaud, S., Tambutté, É., Tambutté, S., Zoccola, D., 2004. Biomineralisation in reef-building corals: from molecular mechanisms to environmental control. Comptes Rendus Palevol 3, 453-467.

Beasley, M.M., Bartelink, E.J., Taylor, L., Miller, R.M., 2014. Comparison of transmission FTIR, ATR, and DRIFT spectra: implications for assessment of bone bioapatite diagenesis. J. Archaeol. Sci 46, 16-22.

Beck, J.W., Edwards, R.L., Ito, E., Taylor, F.W., Recy, J., Rougerie, F., Joannot, P., Henin, C., 1992. Sea-Surface Temperature from Coral Skeletal Strontium/Calcium Ratios. Science 257, 644-647.

Bryan, W.H., D, 1941. Spherulitic crystallization as a mechanism of skeletal growth in the hexacorals. Proceedings of Royal Society of Queensland 52, 78-91.

Cabassi, F., Casu, B., Perlin, A.S., 1978. Infrared absorption and raman scattering of sulfate groups of heparin and related glycosaminoglycans in aqueous solution. Carbohydr. Res. 63, 1-11.

Cael, J.J., Isaac, D.H., Blackwell, J., Koenig, J.L., Atkins, E.D.T., Sheehan, J.K., 1976. Polarized infrared spectra of crystalline glycosaminoglycans. Carbohydr. Res. 50, 169-179.

Campbell, K., MacLennan, D., Jorgensen, A., 1983. Staining of the Ca2+-binding proteins, calsequestrin, calmodulin, troponin C, and S-100, with the cationic carbocyanine dye" Stains-all". J. Biol. Chem. 258, 11267-11273.

Cobb, K.M., Charles, C.D., Cheng, H., Edwards, R.L., 2003. El Nino/Southern Oscillation and tropical Pacific climate during the last millennium. Nature 424, 271-276.

Constantz, B., Weiner, S., 1988. Acidic macromolecules associated with the mineral phase of scleractinian coral skeletons. J. Exp. Zool. 248, 253-258.

Crenshaw, M.A., 1972. The soluble matrix from Mercenaria mercenaria shell. Biomineralization 6, 6-11.

614 Cuif, J., Dauphin, Y., Denis, A., Gautret, P., Marin, F., 1996. The organo-mineral structure of
615 coral skeletons: a potential source of new criteria for Scleractinian taxonomy. Bull.
616 Institut Océanogr. Monaco, Numéro Spécial 14, 4, 359-367.
617 Cuif, J.-P., Dauphin, Y., 2005. The two-step mode of growth in the scleractinian coral
618 skeletons from the micrometre to the overall scale. J. Struct. Biol. 150, 319-331.
619 Cuif, J.-P., Dauphin, Y., Gautret, P., 1999a. Compositional diversity of soluble mineralizing
620 matrices in some recent coral skeletons compared to fine-scale growth structures of
621 fibres: discussion of consequences for biomineralization and diagenesis. International
622 Journal of Earth Sciences 88, 582-592.
623 Cuif, J.-P., Dauphin, Y., Freiwald, A., Gautret, P., Zibrowius, H., 1999b. Biochemical markers
624 of zooxanthellae symbiosis in soluble matrices of skeleton of 24 Scleractinia species.
625 Comparative Biochemistry and Physiology Part A: Molecular & Integrative
626 Physiology 123, 269-278.
627 Cuif, J.P., Dauphin, Y., Doucet, J., Salome, M., Susini, J., 2003. XANES mapping of organic
628 sulfate in three scleractinian coral skeletons. Geochim. Cosmochim. Acta 67, 75-83.
629 Dauphin, Y., 2001. Comparative studies of skeletal soluble matrices from some Scleractinian
630 corals and Molluscs. Int. J. Biol. Macromol. 28, 293-304.
631 Dauphin, Y., Cuif, J.-P., Williams, C.T., 2008. Soluble organic matrices of aragonitic skeletons
632 of Merulinidae (Cnidaria, Anthozoa). Comparative Biochemistry and Physiology Part
633 B: Biochemistry and Molecular Biology 150, 10-22.
634 Drake, J.L., Mass, T., Haramaty, L., Zelzion, E., Bhattacharya, D., Falkowski, P.G., 2013.
635 Proteomic analysis of skeletal organic matrix from the stony coral *Stylophora*
636 *pistillata*. Proc. Natl. Acad. Sci. U. S. A. 110, 3788-3793.
637 Druffel, E.R.M., 1997. Geochemistry of corals: Proxies of past ocean chemistry, ocean
638 circulation, and climate. Proc. Natl. Acad. Sci. U. S. A. 94, 8354-8361.
639 Farre, B., Cuif, J.-P., Dauphin, Y., 2010. Occurrence and diversity of lipids in modern coral
640 skeletons. Zoology 113, 250-257.
641 Gautret, P., Cuif, J.P., Freiwald, A., 1997. Composition of soluble mineralizing matrices in
642 zooxanthellate and non-zooxanthellate scleractinian corals: Biochemical assessment of
643 photosynthetic metabolism through the study of a skeletal feature. Facies 36, 189-194.
644 Hathorne Ed, C., Felis, T., Suzuki, A., Kawahata, H., Cabioch, G., 2013. Lithium in the
645 aragonite skeletons of massive *Porites* corals: A new tool to reconstruct tropical sea
646 surface temperatures. Paleoceanography 28, 143-152.
647 Immel, F., Broussard, C., Catherinet, B., Plasseraud, L., Alcaraz, G., Bundeleva, I., Marin, F.,

2016. The shell of the invasive bivalve species *Dreissena polymorpha*: biochemical, elemental and textural investigations. PLoS One 11, e0154264.

Isa, Y., Okazaki, M., 1987. Some observations on the Ca^{2+}-binding phospholipids from scleractinian coral skeletons. Comp. Biochem. Physiol. B 87, 507-512.

Kanold, J.M., Guichard, N., Immel, F., Plasseraud, L., Corneillat, M., Alcaraz, G., Brümmer, F., Marin, F., 2015. Spine and test skeletal matrices of the Mediterranean sea urchin *Arbacia lixula* – a comparative characterization of their sugar signature. FEBS Journal 282, 1891-1905.

Linsley, B.K., Wellington, G.M., Schrag, D.P., 2000. Decadal Sea Surface Temperature Variability in the Subtropical South Pacific from 1726 to 1997 A.D. Science 290, 1145-1148.

Lloyd, A.G., Dodgson, K.S., Price, R.G., Rose, F.A., 1961. I. Polysaccharide sulphates. Biochim. Biophys. Acta 46, 108-115.

Longas, M.O., Breitweiser, K.O., 1991. Sulfate composition of glycosaminoglycans determined by infrared spectroscopy. Anal. Biochem. 192, 193-196.

Marin, F., Amons, R., Guichard, N., Stigter, M., Hecker, A., Luquet, G., Layrolle, P., Alcaraz, G., Riondet, C., Westbroek, P., 2005. Caspartin and Calprismin, two proteins of the shell calcitic prisms of the Mediterranean fan mussel *Pinna nobilis*. J. Biol. Chem. 280, 33895-33908.

Milliman, J.D., 1993. Production and accumulation of calcium carbonate in the ocean: budget of a nonsteady state. Global Biogeochemical Cycles 7, 927-957.

Mitterer, R.M., 1978. Amino-acid composition and metal-binding capability of skeletal protein of corals. Bull. Mar. Sci. 28, 173-180.

Morrissey, J.H., 1981. Silver stain for proteins in polyacrylamide gels: A modified procedure with enhanced uniform sensitivity. Anal. Biochem. 117, 307-310.

Naggi, A., Torri, G., Iacomi, M., Colombo Castelli, G., Reggi, M., Fermani, S., Dubinsky, Z., Goffredo, S., Falini, G., 2018. Structure and function of stony coral intraskeletal polysaccharides. ACS Omega 3, 2895-2901.

Nudelman, F., Gotliv, B.A., Addadi, L., Weiner, S., 2006. Mollusk shell formation: Mapping the distribution of organic matrix components underlying a single aragonitic tablet in nacre. J. Struct. Biol. 153, 176-187.

Ogilvie, M.M., 1896. Microscopic and systematic study of madreporarian types of corals. Philos. Trans. R. Soc. Lond. B Biol. Sci. 187, 83-345.

Panda, R.N., Hsieh, M.F., Chung, R.J., Chin, T.S., 2003. FTIR, XRD, SEM and solid state

682 NMR investigations of carbonate-containing hydroxyapatite nano-particles
683 synthesized by hydroxide-gel technique. J. Phys. Chem. Solids 64, 193-199.
684 Puverel, S., Tambutte, E., Pererra-Mouries, L., Zoccola, D., Allemand, D., Tambutte, S., 2005.
685 Soluble organic matrix of two Scleractinian corals: Partial and comparative analysis.
686 Comparative Biochemistry and Physiology B-Biochemistry & Molecular Biology 141,
687 480-487.
688 Ramos-Silva, P., Marin, F., Kaandorp, J., Marie, B., 2013a. Biomineralization toolkit: The
689 importance of sample cleaning prior to the characterization of biomineral proteomes.
690 Proc. Natl. Acad. Sci. U. S. A. 110, E2144-E2146.
691 Ramos-Silva, P., Kaandorp, J., Huisman, L., Marie, B., Zanella-Cleon, I., Guichard, N.,
692 Miller, D.J., Marin, F., 2013b. The skeletal proteome of the coral *Acropora millepora*:
693 the evolution of calcification by co-option and domain shuffling. Mol. Biol. Evol. 30,
694 2099-2112.
695 Ramos-Silva, P., Kaandorp, J., Herbst, F., Plasseraud, L., Alcaraz, G., Stern, C., Corneillat,
696 M., Guichard, N., Durlet, C., Luquet, G., Marin, F., 2014. The Skeleton of the
697 Staghorn Coral *Acropora millepora*: Molecular and Structural Characterization. PLoS
698 One 9, e97454.
699 Rivera-Muñoz, E.M., 2011. Hydroxyapatite-Based Materials: Synthesis and Characterization,
700 p. Ch. 04, in: R. Fazel-Rezai, (Ed.), Biomedical Engineering - Frontiers and
701 Challenges, InTech, Rijeka.
702 Rollion-Bard, C., Blamart, D., Trebosc, J., Tricot, G., Mussi, A., Cuif, J.-P., 2011. Boron
703 isotopes as pH proxy: A new look at boron speciation in deep-sea corals using 11B
704 MAS NMR and EELS. Geochim. Cosmochim. Acta 75, 1003-1012.
705 Shinzato, C., Shoguchi, E., Kawashima, T., Hamada, M., Hisata, K., Tanaka, M., Fujie, M.,
706 Fujiwara, M., Koyanagi, R., Ikuta, T., Fujiyama, A., Miller, D.J., Satoh, N., 2011.
707 Using the *Acropora digitifera* genome to understand coral responses to environmental
708 change. Nature 476, 320-U382.
709 Simkiss, K., Wilbur, K.M., 2012. Biomineralization Elsevier.
710 Sondej, M., Denny, P.A., Xie, Y., Ramachandran, P., Si, Y., Takashima, J., Shi, W., Wong,
711 D.T., Loo, J.A., Denny, P.C., 2009. Glycoprofiling of the Human Salivary Proteome.
712 Clin. Proteomics 5, 52-68.
713 Spalding, M., Ravilious, C., Green, E.P., 2001. World atlas of coral reefs Univ of California
714 Press.
715 Takeuchi, T., Yamada, L., Shinzato, C., Sawada, H., Satoh, N., 2016. Stepwise evolution of

716 coral biomineralization revealed with genome-wide proteomics and transcriptomics.
717 PLoS One 11, e0156424.
718 Tambutté, S., Holcomb, M., Ferrier-Pagès, C., Reynaud, S., Tambutté, É., Zoccola, D.,
719 Allemand, D., 2011. Coral biomineralization: From the gene to the environment. J.
720 Exp. Mar. Bio. Ecol. 408, 58-78.
721 Thornton, D.J., Carlstedt, I., Sheehan, J.K., 1996. Identification of glycoproteins on
722 nitrocellulose membranes and gels. Mol. Biotechnol. 5, 171-176.
723 Watanabe, T., Suzuki, A., Minobe, S., Kawashima, T., Kameo, K., Minoshima, K., Aguilar,
724 Y.M., Wani, R., Kawahata, H., Sowa, K., Nagai, T., Kase, T., 2011. Permanent El Nino
725 during the Pliocene warm period not supported by coral evidence. Nature 471, 209-
726 211.
727 Weiner, S., Hood, L., 1975. Soluble protein of the organic matrix of mollusk shells: a potential
728 template for shell formation. Science 190, 987-989.
729 Wild, C., Woyt, H., Huettel, M., 2005. Influence of coral mucus on nutrient fluxes in
730 carbonate sands. Mar. Ecol. Prog. Ser. 287, 87-98.
731

Table 1. Quantification of AIMs and ASMs extracted from *P. australiensis* skeleton.

	AIM ($mg \cdot g^{-1}$)	ASM ($mg \cdot g^{-1}$)	Total organic matrix (% w/w)
2nd bleaching	1.31	0.12 ± 0.01	0.143
3rd bleaching	0.64	0.06 ± 0.01	0.07

732

733

Table 2. CHNS analysis of 3rd bleaching AIM.

	N (wt%)	C (wt%)	H (wt%)	S (wt%)
3bl AIM	1.42	21.63	3.15	1.05

734

735

Figure Legends

Figure 1. SEM images of *Porites australiensis* skeleton before and after second bleaching. (A) Surface of a skeleton fragment before the second bleaching. Fibrous structures of microorganisms (red arrowheads) are visible. (B) The same skeleton surface of (A) after the second bleaching. Contaminating fibers were completely removed. (C) Magnified image of (A). (D) Magnified image of (B).

Figure 2. SDS-PAGE of skeletal organic matrices. (A) Silver staining, (B) Stains-all staining, (C) Alcian blue staining. Twenty µl of sample solution was loaded in each lane for silver staining and 15 µl for Stains-all staining and Alcian blue staining. ASM: Acid-soluble matrix. LS-AIM: Laemmli-soluble acid-insoluble matrix. 2bl: second bleaching. 3bl: third bleaching. MM: Molecular weight markers.

Figure 3. FT-IR spectra of skeletal organic matrices. Major peaks discussed in the main text are colored. These signals indicate the presence of proteins or saccharides (i), lipids (ii), sulphates (iii), phosphates (iv), and saccharides (v). ASM: Acid-soluble matrix. AIM: Acid-insoluble matrix. 2bl: second bleaching. 3bl: third bleaching.

Figure 4. SEM images of $CaCO_3$ crystal formed in the presence of *Porites* ASM. (A-F) Second bleaching ASM: 1µg·mL^{-1} (A), 4µg·mL^{-1} (B), 16µg·mL^{-1} (C,D), 32µg·mL^{-1} (E,F). (G-I) Third bleaching ASM: 1µg·mL^{-1} (G), 4µg·mL^{-1} (H), 16µg·mL^{-1} (I,J), 32µg·mL^{-1} (K,L). (M) $CaCO_3$ crystals generated in ASM-free solution. Morphology of the generated crystals are affected by the presence of ASM in dose-dependent manner. The effect of third bleaching ASM is more pronounced than that of second bleaching ASM.

Figure 5. Monosaccharide composition of ASM and AIM after two (left) or three (right) bleachings. While the third bleaching did not produce any important change in the relative percentages of monosaccharides in AIMS, it was more effective for ASMs, where it induced a noticeable decrease of arabinose percentage.

Figure 6. Enzyme-linked lectin assay (ELLA) on ASMs. ELLA was performed with 21 lectins after the second (left) and third (right) bleaching steps. Absorbance values at 405 nm were normalized to the highest value (DSL), corresponding to 100% reactivity (n = 3, means

770 ± S.D.).
771
772 **Figure 7. *In situ* localization of the DSL-reactive saccharide fraction.** Observation with
773 SEM in secondary electron (SE, A and H) and in back-scattered electron (BSE, B to G)
774 modes. A to F: positive control, with *Datura stramonium* lectin (DSL). G, H: negative control,
775 in the absence of DSL, but with gold-coupled anti-biotin. In (A) and (B), tips of needle-like
776 crystals point to the early mineralization zone (front side of the pictures). The early
777 mineralization zone is indicated in dotted circle in (C). Note that the gold particles,
778 characterized by tiny bright spots in BSE mode, are distributed evenly on the aragonite fibers.
779
780
781

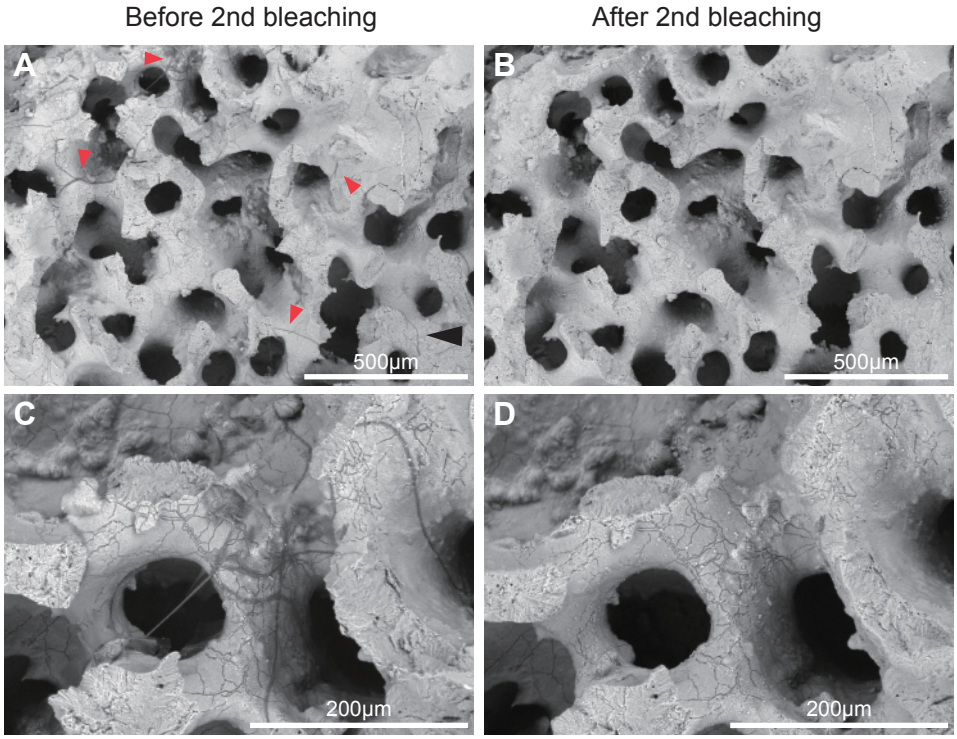
Before 2nd bleaching
After 2nd bleaching
A
B
500μm
500μm
C
D
200μm
200μm

Figure 1.

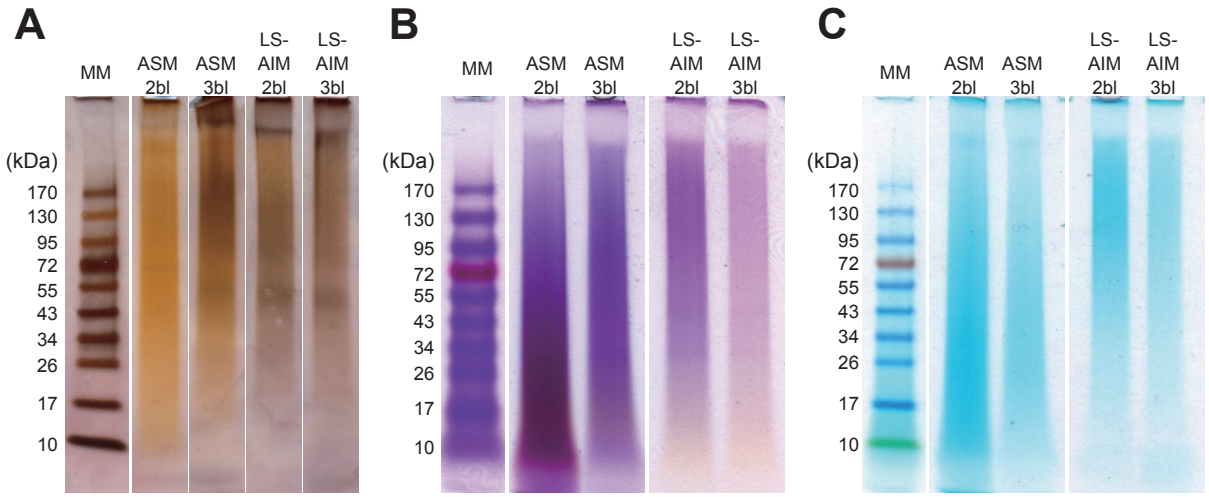
A
MM
ASM 2bl
ASM 3bl
LS-AIM 2bl
LS-AIM 3bl
(kDa)
170
130
95
72
55
43
34
26
17
10
B
MM
ASM 2bl
ASM 3bl
LS-AIM 2bl
LS-AIM 3bl
(kDa)
170
130
95
72
55
43
34
26
17
10
C
MM
ASM 2bl
ASM 3bl
LS-AIM 2bl
LS-AIM 3bl
(kDa)
170
130
95
72
55
43
34
26
17
10

Figure 2.

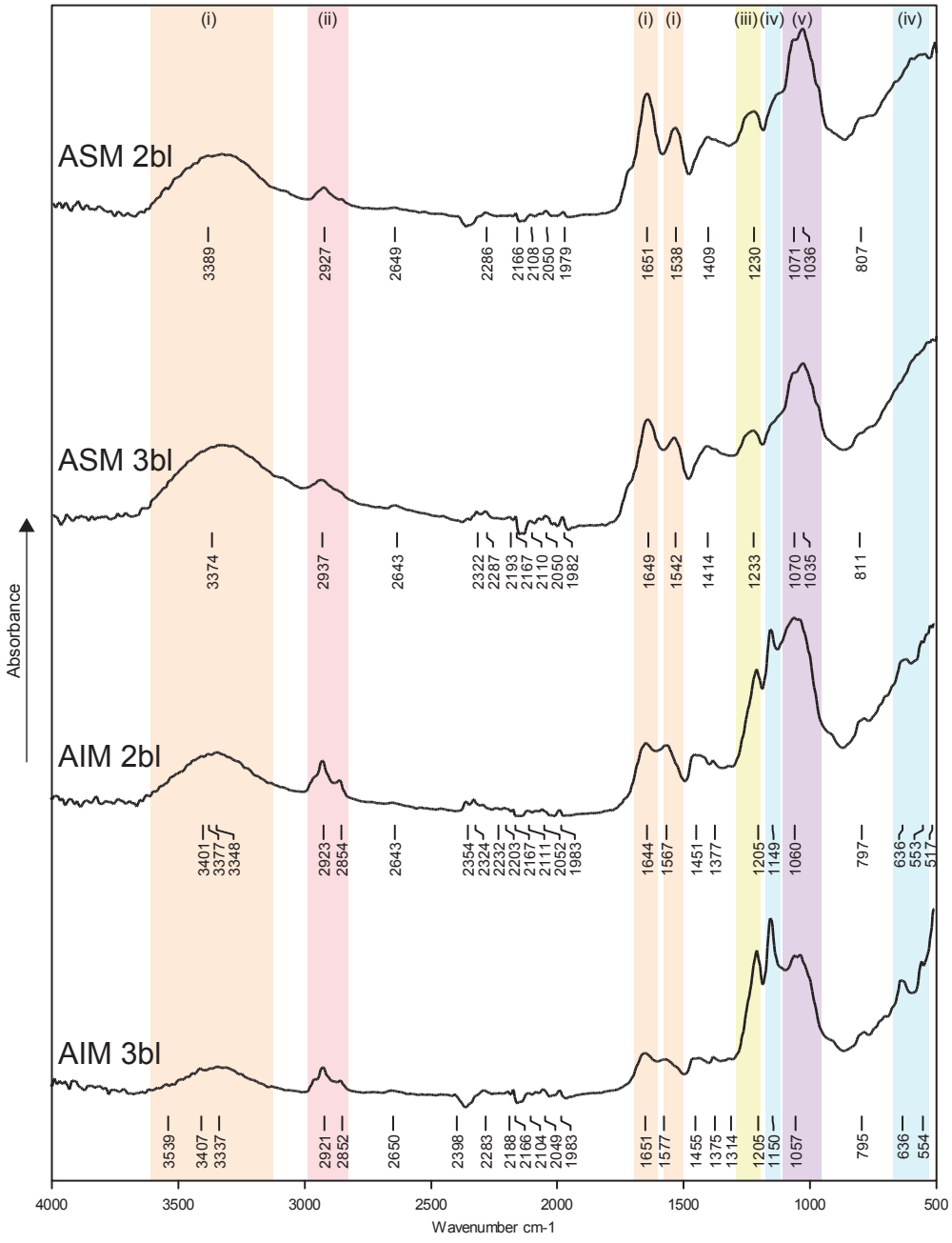
(i)
(ii)
(i)
(i)
(iii)
(iv)
(v)
(iv)
ASM 2bl
3389
2927
2649
2286
2166
2108
2050
1979
1651
1538
1409
1230
1071
1036
807
ASM 3bl
3374
2937
2643
2322
2287
2193
2167
2110
2050
1982
1649
1542
1414
1233
1070
1035
811
AIM 2bl
3401
3377
3348
2923
2854
2643
2354
2324
2232
2203
2167
2111
2052
1983
1644
1567
1451
1377
1205
1149
1060
797
636
553
517
AIM 3bl
3539
3407
3337
2921
2852
2650
2398
2283
2188
2166
2104
2049
1983
1651
1577
1455
1375
1314
1205
1150
1057
795
636
554
Absorbance
4000
3500
3000
2500
2000
1500
1000
500
Wavenumber cm-1

Figure 3.

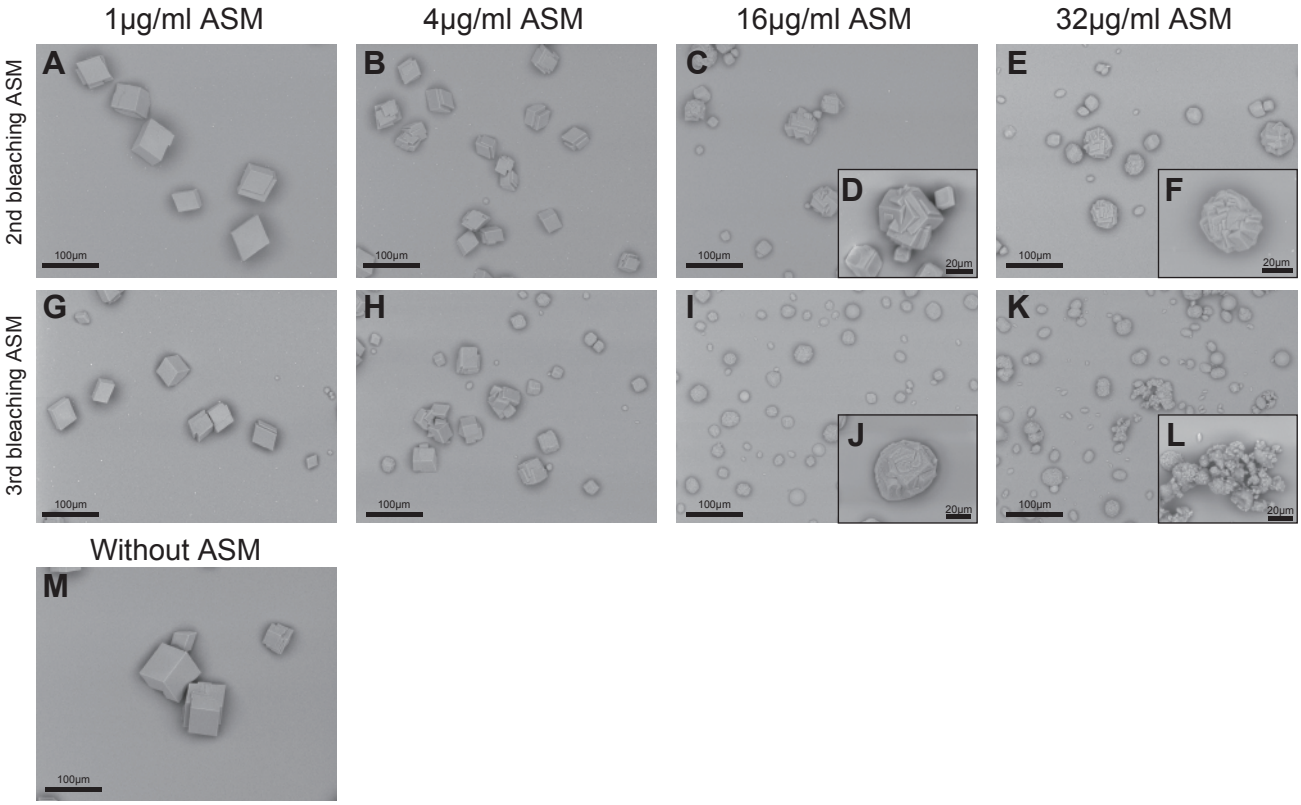
1μg/ml ASM
4μg/ml ASM
16μg/ml ASM
32μg/ml ASM
2nd bleaching ASM
3rd bleaching ASM
A
B
C
D
E
F
G
H
I
J
K
L
M
100μm
20μm
Without ASM

Figure 4.

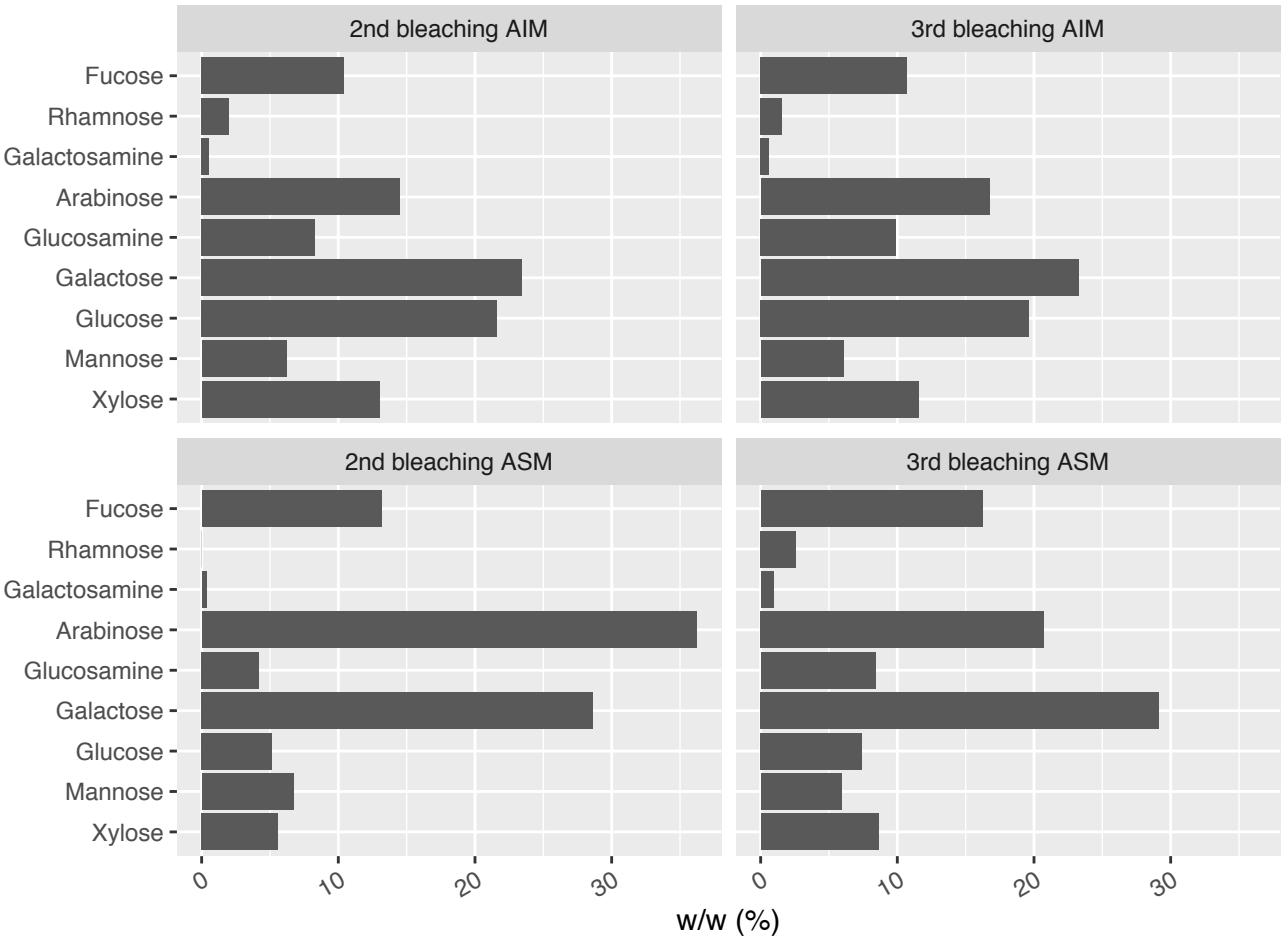
2nd bleaching AIM
3rd bleaching AIM
2nd bleaching ASM
3rd bleaching ASM
Fucose
Rhamnose
Galactosamine
Arabinose
Glucosamine
Galactose
Glucose
Mannose
Xylose
0
10
20
30
w/w (%)

Figure 5.

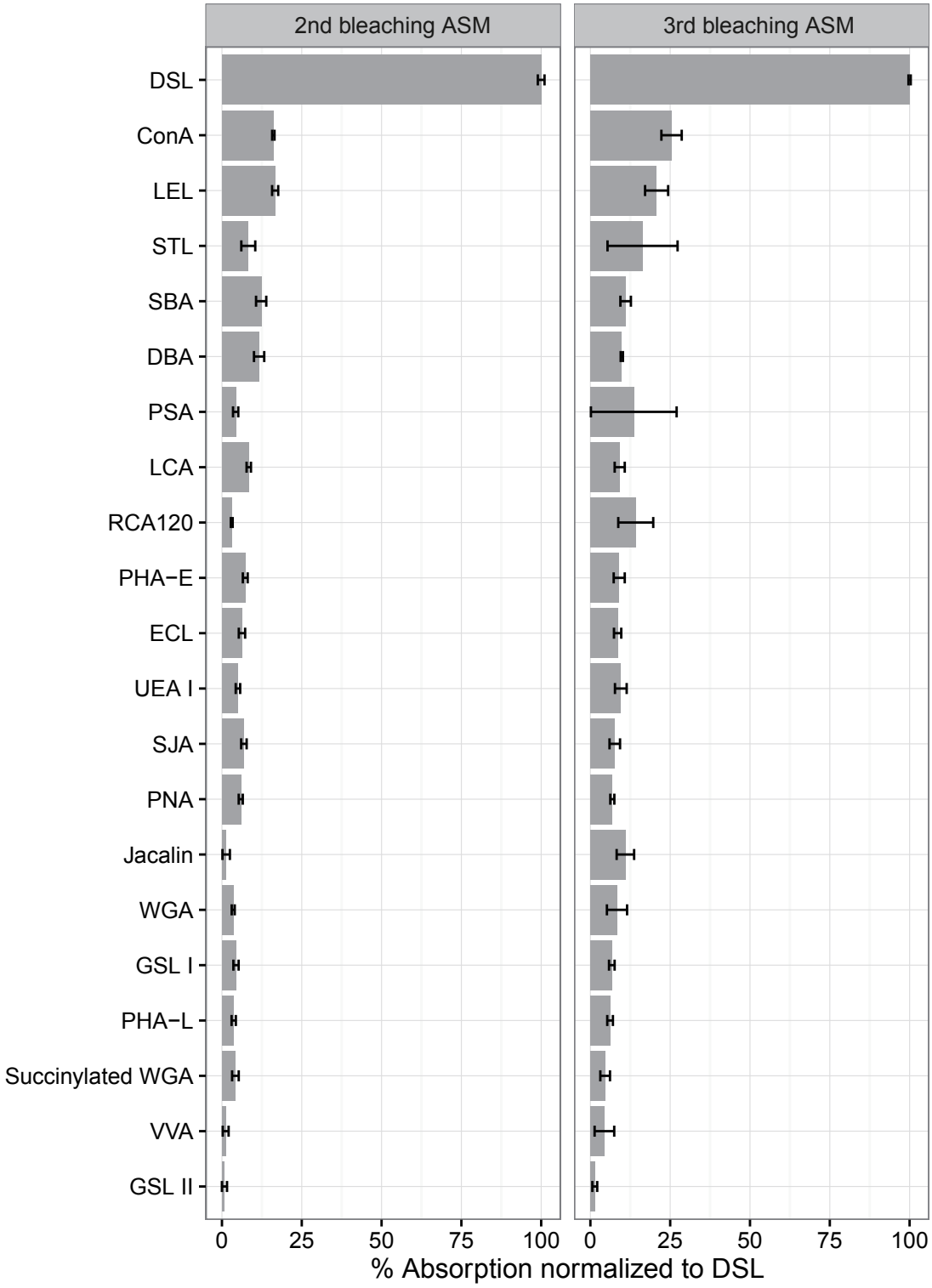
2nd bleaching ASM
3rd bleaching ASM
DSL
ConA
LEL
STL
SBA
DBA
PSA
LCA
RCA120
PHA−E
ECL
UEA I
SJA
PNA
Jacalin
WGA
GSL I
PHA−L
Succinylated WGA
VVA
GSL II
0
25
50
75
100
% Absorption normalized to DSL

Figure 6.

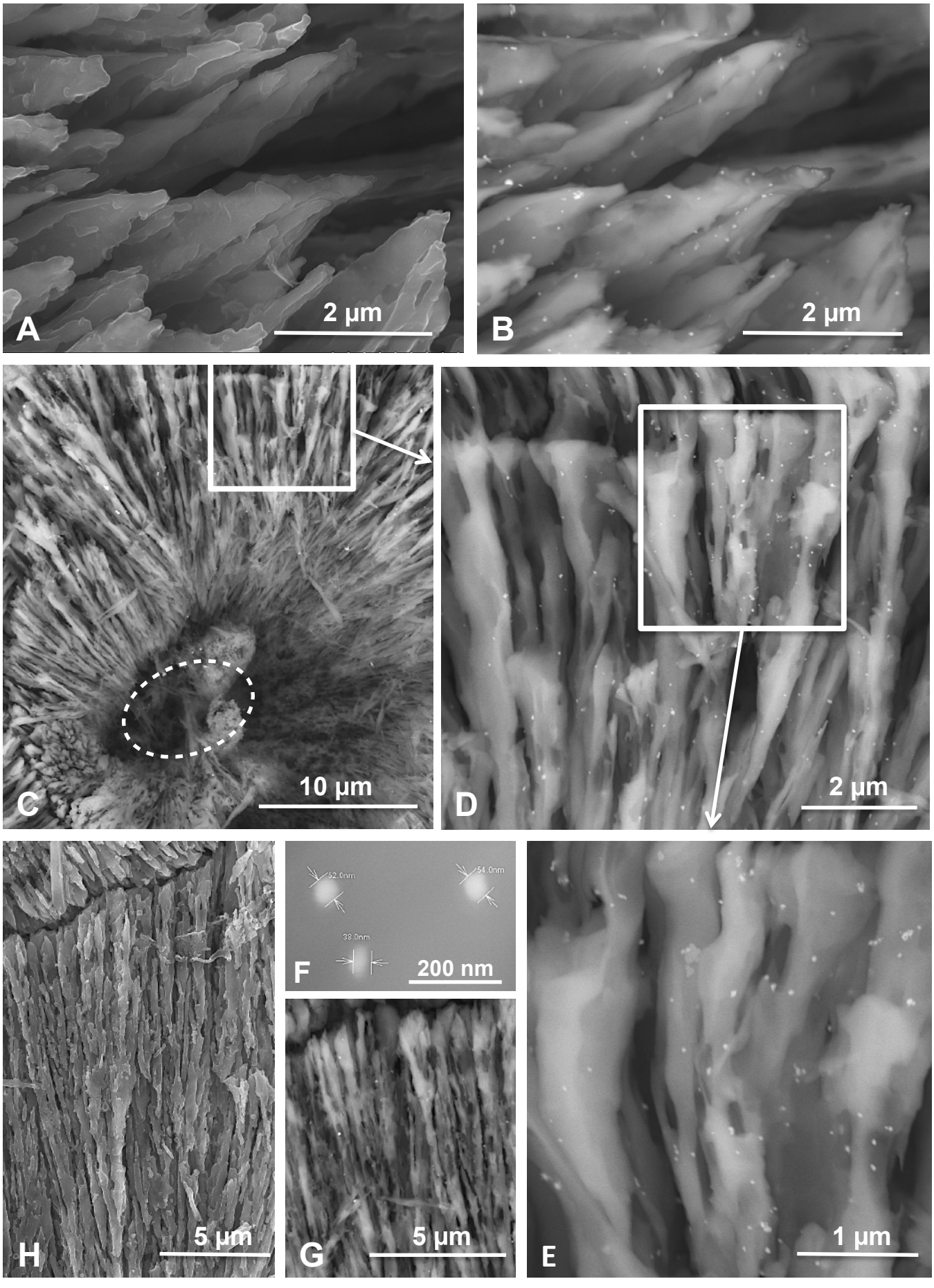
A
2 µm
B
2 µm
C
10 µm
D
2 µm
H
5 µm
F
52.0nm
54.0nm
38.0nm
200 nm
G
5 µm
E
1 µm

Figure 7.